Statistics of Higher-Order Modal Dispersion in Multi-Mode Fiber With Strong Mode Coupling

Anirudh Vijay, *Member, IEEE*, Nika Zahedi, Oleksiy Krutko, *Member, IEEE*, Rebecca Refaee, and Joseph M. Kahn, *Life Fellow, IEEE*

***Abstract*—The effects of mode coupling and first-order modal dispersion in mode-division multiplexed multi-mode fiber systems are well studied. However, when modal delays become frequency-dependent, higher-order modal dispersion effects, such as mode-dependent chromatic dispersion, must be incorporated into propagation models. This work investigates the statistical properties of first- and second-order group-delay operators under strong coupling conditions using a multi-section random matrix model, accounting for both intrinsic (uncoupled) group delays and mode-dependent chromatic dispersion. We show that the asymptotic distributions of these operators are determined by the number of sections, the delay spreads of the uncoupled delays, and mode-dependent chromatic dispersion. For typical graded-index multi-mode fibers, the uncoupled group delays have a significantly greater impact than the mode-dependent chromatic dispersion. As a result, the complexity of digital signal processing is ultimately dictated by the statistics of the first-order group-delay operator. Additionally, we derive analytical expressions for the expected intensity pulse response to provide a time-domain perspective on the higher-order effects.**

***Index Terms*—Group-delay operator, higher-order modal dispersion, intensity pulse response, long-haul multi-mode fiber systems, modal dispersion, mode-division multiplexing.**

I. Introduction

SPACE-DIVISION multiplexing (SDM) improves capacity, integration, and power efficiency in long-haul coherent optical communication systems [1], [2], [3]. SDM can be implemented using various methods, including parallel single-mode fibers, uncoupled-core or coupled-core multi-core fibers, or multi-mode fibers (MMFs). Among these options, mode-division multiplexing (MDM) in MMFs is particularly attractive for achieving the highest level of integration [4], enabling amplification using fewer pump modes than signal modes [5].

Practical implementation of long-haul MDM systems over MMFs is dependent on multiple-input multiple-output (MIMO) digital signal processing (DSP) to mitigate the effects of mode coupling and modal dispersion. Modal dispersion, which arises from the frequency dependence of the modal propagation constants, necessitates MIMO equalization with memory. This dispersion is typically characterized by its first-order frequency dependence, known as group delay (GD), and its second-order dependence, known as chromatic dispersion (CD). The average GD across all modes accumulates linearly with link length and corresponds to link latency without impacting DSP complexity. Similarly, the average CD accumulates linearly and can be effectively compensated using fixed single-input single-output digital filters for each mode prior to the MIMO equalizer.

The primary challenge for MIMO DSP arises from mode-dependent modal and chromatic dispersions. The spread in the uncoupled modal GDs can be substantial, leading to a required DSP memory length that can be comparable to or even larger than that needed for average CD compensation [6]. MMF links need strong random coupling to manage the accumulation of GD spread. In the strong coupling regime, the GD spread is calculated using the distribution of the first-order frequency dependence of the dispersion statistics, showing that the standard deviation (STD) of the coupled GDs scales favorably with the square root of the link length, rather than linearly [6]. The interplay between uncoupled GDs and strong random coupling can also generate higher-order dispersion effects. In the Jones matrix representation of the electric field propagation in MMFs, higher-order modal dispersion refers to a super-linear frequency dependence of the phase of the Jones matrix. It can result in depolarization and a nonlinear relationship between the input and output intensities. These effects have been previously investigated in the frequency domain using multi-section fiber field propagation models, but their statistical properties were not derived analytically [7]. A time-domain perspective, which inherently incorporates these higher-order effects, has also been explored through studies of the intensity impulse response [8]. In these prior works, the models for uncoupled propagation are first-order in frequency and incorporate uncoupled modal group delays, and higher-order frequency dependence emerges as a consequence of random coupling between modes. This is a limitation, as the models do not consider the intrinsic higher-order frequency dependence of the uncoupled modes.

While the intrinsic higher-order frequency dependence of the uncoupled modes may be weak, a thorough statistical investigation of the resulting coupled higher-order dispersion is of fundamental interest. In particular, it is useful to obtain closed-form expressions for the variances of the statistical distributions and

Received 19 August 2025; revised 10 November 2025 and 3 January 2026; accepted 6 January 2026. Date of publication 14 January 2026; date of current version 16 March 2026. This work was supported in part by Ciena Corporation, in part by Stanford Shoucheng Zhang Graduate Fellowship, and in part by Stanford Graduate Fellowship. *(Corresponding author: Anirudh Vijay.)*

The authors are with the E.L Ginzton Laboratory, Department of Electrical Engineering, Stanford University, Stanford, CA 94305 USA (e-mail: avijay@alumni.stanford.edu; nzahedi@stanford.edu; oleksiyk@alumni.stanford.edu; becca24@stanford.edu; jmk@ee.stanford.edu).

Color versions of one or more figures in this article are available at https://doi.org/10.1109/JLT.2026.3654018.

Digital Object Identifier 10.1109/JLT.2026.3654018

study how they depend on fiber properties and other system attributes. This becomes particularly relevant for next-generation systems operating with large signal bandwidths (>100 GHz) or in links where the first-order GD spread has been minimized through advanced fiber and link design, such as graded-index fibers with low differential mode delay or links employing GD compensation techniques. In such systems, where the goal is to reduce DSP complexity as much as possible, it is important to quantify the contribution of the intrinsic higher-order frequency dependence of the uncoupled modes. It is thus far unclear if the coupled higher-order effects, including those arising from uncoupled mode-dependent chromatic dispersion (MDCD), directly influence the required DSP complexity and overall system feasibility.

In this paper, we conduct a theoretical and numerical investigation into the statistics of higher-order modal dispersion in MMFs operating in the strong coupling regime. We analyze the dispersion effects resulting from the combination of uncoupled GDs and MDCD. Starting with the first-order and second-order GD operators, we derive novel analytical expressions for the statistics of their respective eigenvalues, namely, the coupled GD and coupled MDCD. We demonstrate how the coupled MDCD scales with the length of the fiber link. Specifically, we show that the coupled MDCD variance consists of two additive components, one that depends on the square of the uncoupled MDCD variance and scales linearly with the link length, and the other that depends on the uncoupled GD variance and scales quadratically with the link length. We validate our analytical expressions through extensive numerical simulations based on multi-section propagation models. We show that for typical values of uncoupled MDCD in practical MMFs, the statistics of modal dispersion are mainly governed by that of the uncoupled GDs, and as a result, the required MIMO DSP complexity is not influenced by uncoupled MDCD. Similar conclusions can be drawn for coupled-core multi-core fibers (CC-MCFs), as their uncoupled MDCD is expected to be lower than that in MMFs owing to the inherent symmetry of the modes. Furthermore, we provide a time-domain perspective by examining the impact of these higher-order effects on the intensity pulse response.

The remainder of this paper is organized as follows. Section II presents a field-coupling multi-section random matrix model for signal propagation in MMF. Section III defines the first- and second-order GD operators and provides the analytical expressions for STDs of the coupled GD and coupled MDCD in the strong-coupling regime. Section IV provides a brief overview of the intensity pulse response. Section V presents the discussion and conclusions of this work.

II. Multi-Section Random Matrix Model for Signal Propagation

Signal propagation in MMFs can be described by Jones matrix field coupling models [9], [10]. An MMF supporting D spatial and polarization modes of length L may be divided into K sections of length $\Delta L = L/K$, each modeled by a $D \times D$ complex-valued matrix describing electric field transfer. The section length corresponds to the characteristic coupling length associated with strong random coupling due to random perturbations in the fiber and deterministic coupling due to devices like mode scramblers and permuters [10], [11]. Let the transfer matrices of the sections be denoted by $\mathbf{M}_1(\omega_0+\omega), \mathbf{M}_2(\omega_0+\omega), \ldots, \mathbf{M}_K(\omega_0+\omega)$. These are frequency-dependent random matrices at angular frequency ω away from the center frequency ω_0. We are interested in the statistical properties of modal dispersion and thus, we ignore any mode-dependent loss or gain. Assuming strong random coupling, the kth section can be represented by

$$\mathbf{M}_k(\omega_0+\omega) = \mathbf{V}_k \mathbf{\Lambda}_k(\omega_0+\omega)\mathbf{U}_k^H \tag{1}$$

where H denotes Hermitian conjugate, $\mathbf{U}_k$ and $\mathbf{V}_k$ are frequency-independent random unitary matrices representing the input and output mode coupling of the kth section, and $\mathbf{\Lambda}_k(\omega_0+\omega)$ is a diagonal matrix describing uncoupled modal dispersion:

$$\mathbf{\Lambda}_k[i,i](\omega_0+\omega) = \exp\left(\jmath\omega\tau_{k,i}(\omega_0) + \frac{\jmath}{2}\omega^2\eta_{k,i}(\omega_0)\right), \tag{2}$$

where $\jmath = \sqrt{-1}$, and $\tau_{k,i}(\omega_0)$ and $\eta_{k,i}(\omega_0)$ are the uncoupled GD (measured in seconds) and uncoupled MDCD (measured in seconds squared) of the ith mode in the kth fiber section, respectively, at the center frequency ω_0. In the strong coupling regime, the section length corresponds to a characteristic coupling length, and $\mathbf{U}_k$ and $\mathbf{V}_k$ are modeled by independent random unitary matrices. While the model is valid whether or not the uncoupled GDs and MDCDs are the same for different sections, for mathematical simplicity, we assume the sections are statistically identical; for $k = 1, \ldots, K$, $\tau_{k,i}(\omega_0) = \tau_i$ and $\eta_{k,i}(\omega_0) = \eta_i$. Without loss of generality, we assume $\sum_{i=1}^{D} \tau_i = 0$ and $\sum_{i=1}^{D} \eta_i = 0$, i.e., we ignore the mode-averaged GD and CD.

The end-to-end link transfer matrix can be written as the product of the transfer matrices of the K sections:

$$\mathbf{M}(\omega_0+\omega) = \mathbf{M}_K(\omega_0+\omega)\mathbf{M}_{K-1}(\omega_0+\omega)\ldots\mathbf{M}_1(\omega_0+\omega). \tag{3}$$

III. Statistics of Group-Delay Operators

Following [7], [12], we can write an exponential expansion of the end-to-end transfer matrix:

$$\mathbf{M}(\omega_0+\omega) = \mathbf{M}(\omega_0)\, e^{\jmath\omega\mathbf{G}^{(1)}(\omega_0)} e^{\frac{1}{2}\jmath\omega^2\mathbf{G}^{(2)}(\omega_0)} \cdots, \tag{4}$$

where $\mathbf{M}(\omega_0)$ is the zeroth-order propagation operator evaluated at ω_0, and $\mathbf{G}^{(1)}(\omega_0)$ and $\mathbf{G}^{(2)}(\omega_0)$ are the first- and second-order GD operators defined as follows:

$$\mathbf{G}^{(1)} = -\jmath\mathbf{M}^H(\omega_0)\,\mathbf{M}'(\omega_0), \tag{5}$$

$$\mathbf{G}^{(2)} = -\jmath\left(\mathbf{G}^{(1)}(\omega_0)\right)^2 - \jmath\mathbf{M}^H(\omega_0)\,\mathbf{M}''(\omega_0), \tag{6}$$

where $\mathbf{M}'(\omega_0) = \frac{d}{d\omega}\mathbf{M}(\omega_0+\omega)|_{\omega=0}$ and $\mathbf{M}''(\omega_0) = \frac{d^2}{d\omega^2}\mathbf{M}(\omega_0+\omega)|_{\omega=0}$. The eigenvalues of $\mathbf{G}^{(1)}(\omega_0)$ and $\mathbf{G}^{(2)}(\omega_0)$ are the coupled GDs (measured in seconds) and coupled MDCDs (measured in seconds squared) for a narrow-band signal centered at ω_0, respectively. We use (5) and (6) to analytically compute the statistics of coupled GDs and MDCDs in the strong coupling regime for large K.

A. First-Order Group-Delay Operator

Following the concatenation rules for the GD operator in [10], [13], (5) can be expanded in terms of the GD operators of the individual sections. Using (3) and (5), we get

$$\begin{aligned}\mathbf{G}^{(1)} &= \mathbf{G}_1^{(1)} + \mathbf{M}_1^H \mathbf{G}_2^{(1)} \mathbf{M}_1 + \cdots \\ &\quad + \mathbf{M}_1^H \ldots \mathbf{M}_{K-1}^H \mathbf{G}_k^{(1)} \mathbf{M}_{K-1} \ldots \mathbf{M}_1 \\ &= \sum_{k=1}^{K} \mathbf{M}_1^H \ldots \mathbf{M}_{k-1}^H \mathbf{G}_k^{(1)} \mathbf{M}_{k-1} \ldots \mathbf{M}_1, \end{aligned} \tag{7}$$

where the frequency index ω_0 has been omitted for clarity and $\mathbf{G}_k^{(1)}(\omega_0) = -\jmath \mathbf{M}_k^H(\omega_0)\mathbf{M}_k'(\omega_0), k = 1, \ldots, K$. From (1), for $k = 1, \ldots, K$, we obtain

$$\mathbf{G}_k^{(1)}(\omega_0) = -\jmath \mathbf{U}_k \mathbf{\Lambda}_k'(\omega_0) \mathbf{U}_k^H, \tag{8}$$

where $\mathbf{\Lambda}_k'(\omega_0) = \jmath \cdot \mathrm{diag}\{\tau_1, \ldots, \tau_D\}$. As expected, $\mathbf{G}_k^{(1)}$ depends on the uncoupled GDs of the section and is independent of the uncoupled MDCDs.

Prior studies have established that $\mathbf{G}^{(1)}$ is a zero-trace Gaussian unitary ensemble (GUE) [6]. Here, we briefly discuss the reasoning behind this conclusion. Each of the K matrices in the summation in (7) has statistically identical eigenvalues. However, their eigenvectors are independent and identically distributed (IID). As $\mathbf{G}^{(1)}$ is the sum of IID random matrices, and given that each of these matrices has a zero trace, owing to the assumptions that $\sum_{i=1}^{D} \tau_i = 0$ and $\sum_{i=1}^{D} \eta_i = 0$, we can apply the central limit theorem. Thus, $\mathbf{G}^{(1)}$ converges to a zero-trace GUE. It can be shown that the STD of the eigenvalues is given by

$$\sigma_{\mathrm{GD}} = \sqrt{\frac{\mathbb{E}\left\{\mathrm{tr}\mathbf{G}^{(1)^2}\right\}}{D}}, \tag{9}$$

where tr $(\cdot)$ represents the matrix trace, the expectation is over all random realizations of the channel, and

$$\sigma_{\mathrm{GD}}^2 = \frac{K}{D} \sum_{i=1}^{D} \tau_i^2 = K\sigma_\tau^2, \tag{10}$$

where σ_τ is the STD of uncoupled GDs of one section. The coupled GD variance scales linearly with the number of sections, is proportional to the variance of the uncoupled GDs, and is independent of the uncoupled MDCDs.

B. Second-Order Group-Delay Operator

Similarly, the second-order GD operator in (6) can be expanded in terms of the GD operators of the individual sections. Using (3) and (6), we get (11) shown at the bottom of this page, where cc represents the complex conjugate transpose of the preceding product of matrices.

The expression for $\mathbf{G}^{(2)}$ in (11) contains two summations. The first includes K terms dependent on $\mathbf{G}_1^{(2)}, \ldots, \mathbf{G}_K^{(2)}$, and the second includes $K(K-1)/2$ terms dependent on pairwise combinations of $\mathbf{M}_l'$ and $\mathbf{M}_k'$. Invoking arguments similar to those in Section III-A, we can show that $\mathbf{G}^{(2)}$ also converges to a zero-trace GUE. The STD of the eigenvalues is given by

$$\sigma_{\mathrm{MDCD}} = \sqrt{\frac{\mathbb{E}\left\{\mathrm{tr}\mathbf{G}^{(2)^2}\right\}}{D}}, \tag{12}$$

where the expectation is over all random realizations of the channel and

$$\begin{aligned}\sigma_{\mathrm{MDCD}}^2 &= \frac{K}{D} \sum_{i=1}^{D} \eta_i^2 + \frac{K(K-1)}{D^2} \left(\sum_{i=1}^{D} \tau_i^2 \right)^2 \\ &= K\sigma_\eta^2 + K(K-1)\sigma_\tau^4, \end{aligned} \tag{13}$$

where σ_η is the STD of uncoupled MDCDs of one section. Detailed derivation is provided in Appendix A.

Equation (13) shows the contributions of both uncoupled GDs and uncoupled MDCDs to the statistics of coupled MDCDs. The MDCD variance shows a linear K dependence with the uncoupled MDCD variance per section σ_η^2 and a quadratic $K(K-1)$ dependence with the square of the uncoupled GD variance per section σ_τ^4. This implies that at longer link lengths, coupled MDCD statistics will be dominated by the statistics of the uncoupled GDs.

C. Multi-Section Simulations

In this subsection, we present numerical multisection simulations similar to [14] to verify the analytical expressions for σ_{GD} and σ_{MDCD}. We consider a case of $D = 12$ modes and $K = 100$ fiber sections. We generate independent random unitary matrices distributed according to the Haar measure to model the fiber coupling matrices $\mathbf{U}_1, \ldots, \mathbf{U}_K, \mathbf{V}_1, \ldots, \mathbf{V}_K$. We choose values of $\tau_1, \ldots, \tau_D$ and $\eta_1, \ldots, \eta_D$ such that $\sum_{i=1}^{D} \tau_i = 0$ and $\sum_{i=1}^{D} \eta_i = 0$. Over 10,000 trials, we numerically compute the end-to-end transfer matrices and the GD operators and record their eigenvalues.

Figs. 1 and 2 plot the normalized coupled GD STD $\sigma_{\mathrm{GD}}/\sigma_\tau$ and the normalized coupled MDCD STD $\sigma_{\mathrm{MDCD}}/\sigma_\eta$, respectively, as a function of the number of sections K for several values of $\sigma_\eta/\sigma_\tau^2$. The plots are on the log-log scale. We see excellent agreement between the estimates from the multi-section simulations and the analytical expressions. In Fig. 1, as expected, the coupled GD STD is proportional to the square root of the number of sections and is the same for all values of $\sigma_\eta/\sigma_\tau^2$. The analytical and simulation curves for the normalized coupled GD STD for each value of $\sigma_\eta/\sigma_\tau^2$ fall on top of each other.

On the other hand, in Fig. 2, when $\sigma_\eta/\sigma_\tau^2 \ll 1$, the coupled MDCD STD is proportional to the number of sections and is dominated by the statistics of uncoupled GD. When $\sigma_\eta/\sigma_\tau^2 \gg 1$, the coupled MDCD STD is proportional to the square root of the number of sections and is dominated by the statistics of

$$\mathbf{G}^{(2)} = \sum_{k=1}^{K} \mathbf{M}_1^H \ldots \mathbf{M}_{k-1}^H \mathbf{G}_k^{(2)} \mathbf{M}_{k-1} \ldots \mathbf{M}_1 - \jmath \sum_{1 \le l < k \le K} \left(\mathbf{M}_1^H \ldots \mathbf{M}_k^H \mathbf{M}_k' \mathbf{M}_{k-1} \ldots \mathbf{M}_{l+1} \mathbf{M}_l' \mathbf{M}_{l-1} \ldots \mathbf{M}_1 - \mathrm{cc} \right). \tag{11}$$

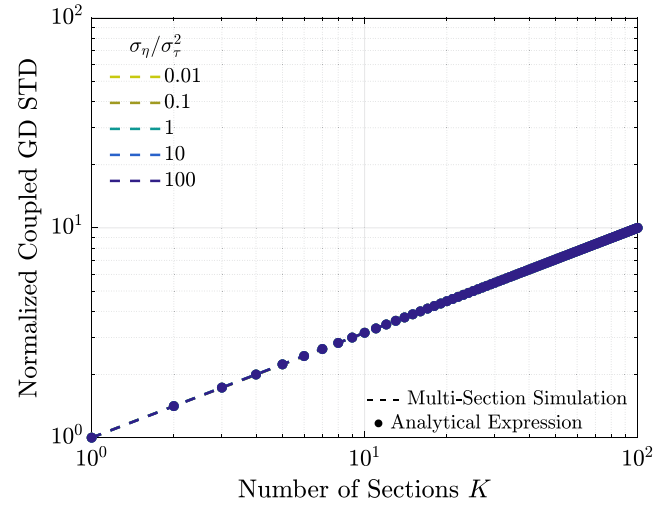

Fig. 1. Coupled GD STD as a function of the number of sections for various values of $\sigma_\eta/\sigma_\tau^2$. The dashed lines correspond to numerical estimates from multi-section simulations and the solid circles correspond to analytical estimates from the formula in (9). Coupled GD STD is normalized by the STD of uncoupled GDs over one section.

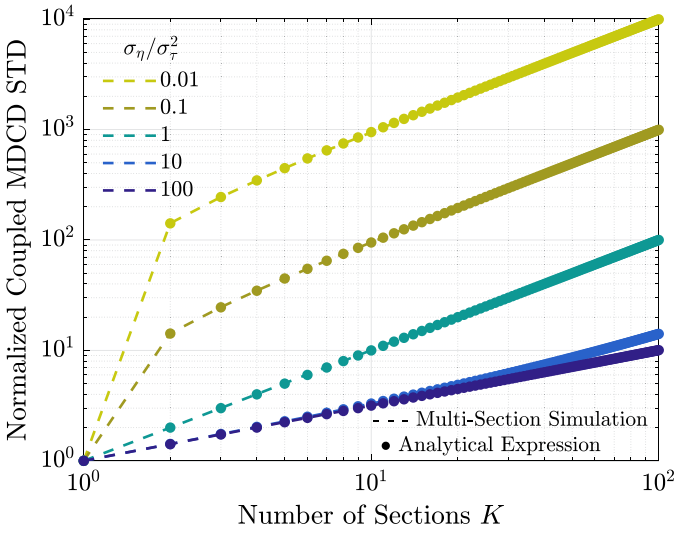

Fig. 2. Coupled MDCD STD as a function of the number of sections for various values of $\sigma_\eta/\sigma_\tau^2$. The dashed lines correspond to numerical estimates from multi-section simulations and the solid circles correspond to analytical estimates from the formula in (12). Coupled MDCD STD is normalized by the STD of uncoupled MDCDs over one section.

uncoupled MDCD. It is also observed that when $\sigma_\eta/\sigma_\tau^2 > 1$, for sufficently large K, the coupled MDCD STD accumulates linearly with K as indicated by the change in the slope of the log-log plot.

In weakly guiding waveguides such as graded-index MMFs, CD is primarily determined by the material properties [15]. Uncoupled MDCDs, unlike the GDs, do not exhibit significant variations due to refractive index perturbations. In typical graded-index MMFs that support few mode groups, the mode-averaged CD parameter is reported to be around $17-21\,\mathrm{ps/nm\cdot km}$ in the C-band, with an uncoupled MDCD of at most $\pm 1\,\mathrm{ps/nm\cdot km}$ [16], [17]. In [16], the uncoupled MDCD STD is $0.26\,\mathrm{ps/nm\cdot km}$ or equivalently, $0.33\,\mathrm{ps^2/km}$. The uncoupled GD STD is reported to be $3.61\,\mathrm{ps/km}$. Assuming a section length of 25 km, we get $\sigma_\eta = 0.26\,\mathrm{ps^2/km}\times 25\,\mathrm{km} = 6.5\,\mathrm{ps^2}$ and $\sigma_\tau = 3.61\,\mathrm{ps/km}\times 25\,\mathrm{km} = 90.25\,\mathrm{ps}$, we find that $\sigma_\eta/\sigma_\tau^2 = 8\times 10^{-4} \ll 1$. Even if the uncoupled MDCD STD were higher, at say $1\,\mathrm{ps^2/km}$, and the uncoupled GD STD lower at $1\,\mathrm{ps/km}$ due to better fiber design or GD compensation, for the same section length we obtain $\sigma_\eta = 1\,\mathrm{ps^2/km}\times 25\,\mathrm{km} = 25\,\mathrm{ps^2}$ and $\sigma_\tau = 1\,\mathrm{ps/km}\times 25\,\mathrm{km} = 25\,\mathrm{ps}$, resulting in $\sigma_\eta/\sigma_\tau^2 = 0.04$ which is still much less than 1. In both cases, the statistics of higher-order modal dispersion are predominantly governed by those of the uncoupled GDs. Also, the memory length requirement for the MIMO DSP is dominated by the effect of the uncoupled GDs, with the effect of the uncoupled MDCDs being negligible. In CC-MCFs, uncoupled MDCD is smaller due to the symmetry of the coupled modes, and therefore, we expect the statistics of higher-order modal dispersion to be predominantly governed by those of the uncoupled GDs.

IV. Intensity Pulse Response

The GD operator-based approach enables us to understand the effects of modal dispersion in the frequency domain. By truncating the exponential expansion of the end-to-end transfer matrix, we obtain an approximation that is valid for narrow-band signals that occupy a frequency range less than the "coherence-bandwidth" of the matrix channel [14], [18]. In the strong coupling regime, for the first-order approximated model, the coherence bandwidth is approximately $1/\sigma_\tau$. A wide-band signal with a bandwidth $W/2\pi$ can be viewed as consisting of $N = \lceil W\sigma_\tau/2\pi \rceil$ sub-bands, each with IID channel realizations. The coupled GDs of each of these sub-bands will also be IID. The statistics of the peak-to-peak delay difference for each of these sub-bands are the same and are well understood [19]. These can help determine the number of taps required for a MIMO DSP filter to equalize the matrix channel [20].

An alternative time-domain approach is through the study of an intensity pulse response (IPR) and has been discussed in the literature [8]. In this section, we briefly study the IPR in the strong coupling regime for the cases with and without uncoupled MDCD. We observe that the pulse spreading due to modal dispersion is not significantly affected by the statistics of uncoupled MDCD for typical values, consistent with observations from the GD operator-based approach in Section III.

The input-output relationship in the time and frequency domains can be written as follows:

$$\mathbf{Y}(\omega) = \mathbf{M}(\omega_0+\omega)\mathbf{X}(\omega) \leftrightarrow y_j(t) = \sum_{i=1}^{D} m_{ji}(t) * x_i(t), \tag{14}$$

where $*$ represents convolution, $\mathbf{X}(\omega) = [X_1(\omega),\ldots,X_D(\omega)]^T$ and $\mathbf{Y}(\omega) = [Y_1(\omega),\ldots,Y_D(\omega)]^T$ are the frequency-domain complex-baseband input and output vectors of modal field amplitudes, $x_i(t) = \mathcal{F}^{-1}\{X_i(\omega)\}, y_i(t) = \mathcal{F}^{-1}\{Y_i(\omega)\}$ are the respective time-domain waveforms, $\mathcal{F}^{-1}\{\cdot\}$ represents the inverse Fourier transform, and $m_{ji}(t)$ is the impulse response of the channel between the ith input mode and the jth output mode.

The intensity is defined in the time domain and frequency domain as follows:

$$i_y(t) = \sum_{j=1}^{D} |y_j(t)|^2 \leftrightarrow$$

$$\mathcal{I}_y(\omega) = \frac{1}{2\pi}\int_{-\infty}^{\infty} \mathbf{X}^H(-\omega')\mathbf{M}^H(\omega_0-\omega') \times \mathbf{M}(\omega_0+\omega-\omega')\mathbf{X}(\omega-\omega')d\omega'. \quad (15)$$

The expected intensity pulse response is given by

$$\mathbb{E}\{\mathcal{I}_y(\omega)\} = \frac{1}{2\pi}\int_{-\infty}^{\infty} \mathbf{X}^H(-\omega')\boldsymbol{\mathcal{H}}(\omega',\omega)\mathbf{X}(\omega-\omega')d\omega', \quad (16)$$

where $\boldsymbol{\mathcal{H}}(\omega',\omega)$ is the autocorrelation of the channel transfer matrix,

$$\boldsymbol{\mathcal{H}}(\omega',\omega) = \mathbb{E}\left\{\mathbf{M}^H(\omega_0-\omega')\mathbf{M}(\omega_0+\omega-\omega')\right\}. \quad (17)$$

From the multisection model (1) and (3), we obtain

$$\mathbf{M}(\omega_0+\omega) = \mathbf{V}_K\boldsymbol{\Lambda}_K(\omega_0+\omega)\mathbf{U}_K^H\mathbf{V}_{K-1}\ldots\boldsymbol{\Lambda}_1(\omega_0+\omega)\mathbf{U}_1^H, \quad (18)$$

which yields

$$\boldsymbol{\mathcal{H}}(\omega',\omega) = \mathbb{E}\Big\{\mathbf{U}_1\boldsymbol{\Lambda}_1^H(\omega_0-\omega')\mathbf{V}_1^H\ldots\boldsymbol{\Lambda}_K^H(\omega_0-\omega') \times \boldsymbol{\Lambda}_K(\omega_0+\omega-\omega')\mathbf{U}_K^H\mathbf{V}_{K-1}\ldots\boldsymbol{\Lambda}_1(\omega_0+\omega-\omega')\mathbf{U}_1^H\Big\}. \quad (19)$$

The expectation can be computed by repeatedly using the property of integration with respect to the Haar measure on the unitary group [21]. We obtain

$$\boldsymbol{\mathcal{H}}(\omega',\omega) = f(\omega',\omega)\mathbf{I}_D, \quad (20)$$

where

$$f(\omega',\omega) = \left(\frac{1}{D}\sum_{j=1}^{D}\exp\left\{\jmath\omega\tau_j - \jmath\omega\omega'\eta_j + \jmath\frac{\omega^2}{2}\eta_j\right\}\right)^K. \quad (21)$$

We observe that $\boldsymbol{\mathcal{H}}(\omega',\omega)$ is a scalar times the identity matrix. In the expected sense, the frequency autocorrelation of the channel matrix is identical for all modes in the strong coupling regime.

1) In the Absence of Uncoupled MDCD: When $\eta_j = 0, j = 1,\ldots,D$, we observe that

$$f(\omega',\omega) = f(0,\omega) = \left(\frac{1}{D}\sum_{j=1}^{D}\exp\jmath\omega\tau_j\right)^K$$

is independent of ω'. This means that the frequency autocorrelation between two different frequencies only depends on the frequency difference. As a result, we obtain

$$\mathbb{E}\{\mathcal{I}_y(\omega)\} = \frac{1}{2\pi}f(0,\omega)\int_{-\infty}^{\infty}\mathbf{X}^H(-\omega')\mathbf{X}(\omega-\omega')d\omega' = f(0,\omega)\mathcal{I}_x(\omega), \quad (22)$$

where $\mathcal{I}_x(\omega)$ is the Fourier transform of the intensity of the input pulse. In (22), $f(0,\omega)$ acts like a frequency response of the channel in transforming the input intensity waveform to the expected output intensity waveform. Therefore, one can define an intensity impulse response, $h(t) = \mathcal{F}^{-1}\{f(0,\omega)\}$, similar to [8].

Here we derive an expression for $f(0,\omega)$ for large K. It is to be noted that $(1/D)\times\sum_{j=1}^{D}\exp\jmath\omega\tau_j$ is the characteristic function of a multinomial random variable with outcomes $\{\tau_1,\ldots,\tau_D\}$. Further, $\{(1/D)\times\sum_{j=1}^{D}\exp\jmath\omega\tau_j\}^K$ is the characteristic function of the sum of K such IID random variables. From the central limit theorem, we know that the distribution of a sum of K IID random variables approaches a Gaussian distribution. Notably, the characteristic function of a Gaussian random variable is also Gaussian. Therefore, in the limit of large K, we obtain

$$f(0,\omega) = \left(\frac{1}{D}\sum_{j=1}^{D}\exp\jmath\omega\tau_j\right)^K \approx \exp\left\{-\frac{K\sigma_\tau^2\omega^2}{2}\right\}, \quad (23)$$

and the time-domain intensity impulse response is also Gaussian with a STD of $\sqrt{K}\sigma_\tau$. This result is consistent with the findings in [8].

2) In the Presence of Uncoupled MDCD: In the general case, when $\eta_j \neq 0, j = 1,\ldots,D$, we do not obtain an intensity impulse response. However, when $\sigma_\eta/\sigma_\tau^2 < 1$, the frequency autocorrelation in (21) is well approximated by a Gaussian function in ω for large K:

$$f(\omega',\omega) \approx \exp\left\{\frac{-K\sigma_\tau^2\omega^2}{2}\left(1+\frac{\sigma_\eta^2}{\sigma_\tau^2}\omega'^2\right)\right\}, \quad (24)$$

where we assume that the uncoupled GDs $\{\tau_i\}$ and the uncoupled MDCDs $\{\eta_i\}$ are uncorrelated. Substituting (24) and (20) in (16) yields (25) shown at the bottom of this page.

There is no closed-form expression for $\mathbb{E}\{\mathcal{I}_y(\omega)\}$ for an arbitrary input waveform. However, assuming that the input electric field is a Nyquist sinc pulse of bandwidth W, $\frac{W}{2\pi}\text{sinc}(\frac{Wt}{2\pi})$, and $K(W\sigma_\tau)^2 \gg 1$, we can further approximate (25) using the following analytical expression:

$$\mathbb{E}\{\mathcal{I}_y(\omega)\} = \frac{1}{2\sqrt{\pi}}\exp\left\{\frac{-K\sigma_\tau^2\omega^2}{2}\right\}\frac{\text{erf}\left(\sqrt{\frac{K}{2}}\frac{\sigma_\eta W\omega}{2}\right)}{\sqrt{\frac{K}{2}}\sigma_\eta\omega}. \quad (26)$$

The time-domain output intensity pulse response can be numerically obtained through an inverse Fourier transform of (26).

3) Multi-Section Simulations: We verify the analytical expressions through multi-section simulations similar to those described in Section III-C. The input pulse is chosen to be $x(t) = \text{sinc}(2t/\sigma_\tau)$, launched in one of the modes and propagated through $K = 100$ sections of a MMF that supports $D = 12$ modes. Figs. 3(a) and 3(b) plot the input intensity and expected output intensity, respectively, for various values

$$\mathbb{E}\{\mathcal{I}_y(\omega)\} \approx \frac{1}{2\pi}\exp\left\{\frac{-K}{2}\sigma_\tau^2\omega^2\right\}\int_{-\infty}^{\infty}\exp\left\{\frac{-K}{2}\sigma_\eta^2\omega'^2\omega^2\right\}\mathbf{X}^H(-\omega')\mathbf{X}(\omega-\omega')d\omega', \quad (25)$$

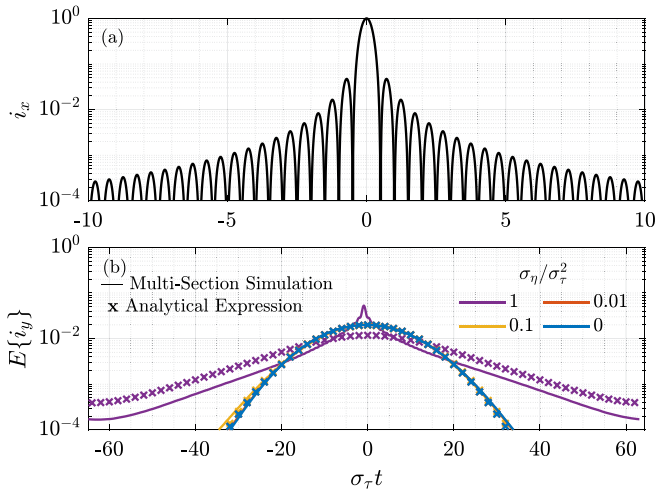

Fig. 3. Intensity pulse response in the presence of strong random mode coupling. (a) Intensity of the Nyquist input pulse, $i_x(t) = \mathrm{sinc}^2(2t/\sigma_\tau)$; (b) Expected output intensity after $K = 100$ sections for various values of $\sigma_\eta/\sigma_\tau^2$. The solid lines correspond to multi-section simulations and the x-markers correspond to the inverse Fourier transform of the analytical expression in (26).

of $\sigma_\eta/\sigma_\tau^2$. The estimates from the analytical expression in (26) are also shown alongside the simulation results in Fig. 3(b). We observe that the estimates from the analytical expression closely align with those from the simulations when $\sigma_\eta/\sigma_\tau^2 < 1$. This is the regime where pulse spreading is primarily influenced by the statistics of uncoupled GDs and the expected output pulse is approximately Gaussian with STD of $\sqrt{K}$ times the uncoupled GD STD. However, the analytical estimates diverge from the simulation results when $\sigma_\eta/\sigma_\tau^2 = 1$, at which point the analytical expression tends to overestimate the pulse spreading. In this regime, the expected output pulse is no longer Gaussian, and the pulse width is greater than $\sqrt{K}\sigma_\tau$. A key takeaway is that for typical values of uncoupled MDCD in graded-index MMFs, i.e., $\sigma_\eta/\sigma_\tau^2 < 0.04$, we observe no significant increase in pulse spreading.

V. Discussion and Conclusion

Strong random mode coupling in MMFs has been viewed as beneficial in reducing the accumulation of GD spread and mode-dependent loss. The frequency decorrelation of the transfer matrix, resulting from the interaction between modal dispersion and strong random mode coupling, is not significantly affected by the intrinsic higher-order frequency dependence of the modal delays. Although this paper only explicitly derives the statistics of the first- and second-order GD operators, we can argue that the statistics of other higher-order GD operators will also be mainly determined by the statistics of the uncoupled GDs and the length of propagation. A practical implication of this study is that the DSP requirements in a long-haul coherent-detection MMF link are dictated by the accumulated coupled GD STD and the average CD at the end of the link. From a system modeling perspective, numerical multi-section models for the strong coupling regime only need to incorporate first-order effects in each section.

In conclusion, we analyzed the phenomenon of coupled modal dispersion resulting from uncoupled GDs and MDCD. We derived analytical expressions for the statistics of the coupled GD and coupled MDCD. We showed that the coupled MDCD variance consists of two additive components: one component corresponds to the uncoupled MDCD variance and scales linearly with the link length, while the other corresponds to the uncoupled GD variance and scales quadratically with the link length. We also provided a time-domain perspective through the intensity pulse response. We found that for typical values of uncoupled MDCD in practical MMFs, the modal dispersion in the strong coupling regime is predominantly influenced by the statistics of uncoupled GD.

Appendix A
Distribution of the Second-Order Group-Delay Operator

In this appendix, we derive the distribution of the second-order GD operator in (11). Using similar arguments to those in Section III-A, it is straightforward to show that the first sum converges to a zero-trace GUE. The variance of the eigenvalues is $(K/D) \cdot \sigma_\eta^2$. The second sum has $K(K-1)/2$ Hermitian matrices of the form

$$\mathbf{A}^H\mathbf{TBTC} + \mathbf{C}^H\mathbf{TB}^H\mathbf{TA}, \tag{27}$$

where $\mathbf{T} = -j\mathbf{\Lambda}' = \mathrm{diag}\{\tau_1, \ldots, \tau_D\}$ is a real-valued deterministic diagonal matrix of delays, and

$$\mathbf{A} = \mathbf{U}_k^H\mathbf{V}_{k-1}\mathbf{U}_{k-1}^H \ldots \mathbf{V}_1\mathbf{U}_1^H,$$
$$\mathbf{B} = \mathbf{U}_k^H\mathbf{V}_{k-1}\mathbf{U}_{k-1}^H \ldots \mathbf{V}_{l+1}\mathbf{U}_{l+1}^H\mathbf{V}_l,$$
$$\mathbf{C} = \mathbf{U}_l^H\mathbf{V}_{l-1}\mathbf{U}_{l-1}^H \ldots \mathbf{V}_1\mathbf{U}_1^H,$$

where $1 \le l < k \le K$, and $\{\mathbf{V}_1, \ldots, \mathbf{V}_K, \mathbf{U}_1, \ldots, \mathbf{U}_K\}$ are IID random unitary matrices, distributed according to the Haar measure. Noting that $\mathbf{A} = \mathbf{BC}$, we can write (27) as

$$\mathbf{C}^H\left(\mathbf{B}^H\mathbf{TBT} + \mathbf{TB}^H\mathbf{TB}\right)\mathbf{C}.$$

Using the fact that the unitary coupling matrices are independent, it can be shown that the second sum in (11) is also a zero-trace GUE. The variance of the eigenvalues is the sum of the variances of each of the matrix terms. The variance of the matrix in (27) is $(1/D)^2 \cdot 2 \cdot \mathrm{tr}\mathbf{T}^2$. This yields us the result in (13).

Acknowledgment

The authors are grateful for helpful discussions with M. O'Sullivan.

References

[1] D. J. Richardson, J. M. Fini, and L. E. Nelson, "Space-division multiplexing in optical fibres," *Nature Photon.*, vol. 7, no. 5, pp. 354–362, May 2013. [Online]. Available: https://www.nature.com/articles/nphoton.2013.94

[2] R.-J. Essiambre and R. W. Tkach, "Capacity trends and limits of optical communication networks," *Proc. IEEE*, vol. 100, no. 5, pp. 1035–1055, May 2012,. [Online]. Available: https://ieeexplore.ieee.org/document/6170861

[3] B. J. Puttnam, G. Rademacher, and R. S. Luís, "Space-division multiplexing for optical fiber communications," *Optica*, vol. 8, no. 9, Sep. 2021, Art. no. 1186. [Online]. Available: https://opg.optica.org/abstract.cfm?URI=optica-8-9-1186

[4] P. J. Winzer, R. Ryf, and S. Randel, "Chapter 10 - spatial multiplexing using multiple-input multiple-output signal processing," in *Optical Fiber Telecommunications* (Optics and Photonics Series), 6th ed, I. P. Kaminow, T. Li, and A. E. Willner, Eds. Boston, MA, USA: Academic Press, Jan. 2013, pp. 433–490. [Online]. Available: https://www.sciencedirect.com/science/article/pii/B9780123969606000109

[5] H. Srinivas, O. Krutko, and J. M. Kahn, "Efficient integrated multimode amplifiers for scalable long-haul SDM transmission," *J. Lightw. Technol.*, vol. 41, no. 15, pp. 4989–5002, Aug. 2023. [Online]. Available: https://ieeexplore.ieee.org/document/10064021/

[6] K.-P. Ho and J. M. Kahn, "Statistics of group delays in multimode fiber with strong mode coupling," *J. Lightw. Technol.*, vol. 29, no. 21, pp. 3119–3128, Nov. 2011. [Online]. Available: https://ieeexplore.ieee.org/document/5986664/

[7] M. Shemirani and J. Kahn, "Higher-order modal dispersion in graded-index multimode fiber," *J. Lightw. Technol.*, vol. 27, no. 23, pp. 5461–5468, Dec. 2009. [Online]. Available: https://ieeexplore.ieee.org/document/5204228/

[8] A. Mecozzi, C. Antonelli, and M. Shtaif, "Intensity impulse response of SDM links," *Opt. Exp.*, vol. 23, no. 5, pp. 5738–5743, Mar. 2015. [Online]. Available: https://opg.optica.org/oe/abstract.cfm?uri=oe-23-5-5738

[9] S. Fan and J. M. Kahn, "Principal modes in multimode waveguides," *Opt. Lett.*, vol. 30, no. 2, pp. 135–137, Jan. 2005. [Online]. Available: https://opg.optica.org/abstract.cfm?URI=ol-30-2-135

[10] K.-P. Ho and J. M. Kahn, "Linear propagation effects in mode-division multiplexing systems," *J. Lightw. Technol.*, vol. 32, no. 4, pp. 614–628, Feb. 2014. [Online]. Available: https://ieeexplore.ieee.org/document/6615972/

[11] S. O. Arik, K.-P. Ho, and J. M. Kahn, "Delay spread reduction in mode-division multiplexing: Mode coupling versus delay compensation," *J. Lightw. Technol.*, vol. 33, no. 21, pp. 4504–4512, Nov. 2015. [Online]. Available: https://ieeexplore.ieee.org/document/7234843/

[12] A. Eyal, W. Marshall, M. Tur, and A. Yariv, "Representation of second-order polarisation mode dispersion," *Electron. Lett.*, vol. 35, no. 19, pp. 1658–1659, Sep. 1999. [Online]. Available: https://digital-library.theiet.org/doi/10.1049/el%3A19991136

[13] H. Kogelnik, R. M. Jopson, and L. E. Nelson, "Chapter 15 - polarization-mode dispersion," in *Optical Fiber Telecommunications IV-B* (Optics and Photonics Series), 4th ed, I. P. Kaminow and T. Li, Eds. Burlington, NJ, USA: Academic Press, Jan. 2002, pp. 725–861. [Online]. Available: https://www.sciencedirect.com/science/article/pii/B9780123951731500153

[14] K.-P. Ho and J. M. Kahn, "Frequency diversity in mode-division multiplexing systems," *J. Lightw. Technol.*, vol. 29, no. 24, pp. 3719–3726, Dec. 2011. [Online]. Available: https://ieeexplore.ieee.org/document/6060841/

[15] M. DiDomenico, "Material dispersion in optical fiber waveguides," *Appl. Opt.*, vol. 11, no. 3, pp. 652–654, Mar. 1972. [Online]. Available: https://opg.optica.org/ao/abstract.cfm?uri=ao-11-3-652

[16] P. Sillard, M. Bigot-Astruc, and D. Molin, "Few-mode fibers for mode-division-multiplexed systems," *J. Lightw. Technol.*, vol. 32, no. 16, pp. 2824–2829, Aug. 2014. [Online]. Available: https://ieeexplore.ieee.org/document/6778763/?arnumber=6778763

[17] P. Sillard et al., "Low-differential-mode-group-delay 9-LP-mode fiber," *J. Lightw. Technol.*, vol. 34, no. 2, pp. 425–430, Jan. 2016. [Online]. Available: https://ieeexplore.ieee.org/document/7174947

[18] J. Carpenter, B. J. Eggleton, and J. Schröder, "Observation of Eisenbud–Wigner–Smith states as principal modes in multimode fibre," *Nature Photon.*, vol. 9, no. 11, pp. 751–757, Nov. 2015. [Online]. Available: https://www.nature.com/articles/nphoton.2015.188

[19] K.-P. Ho and J. M. Kahn, "Chapter 11 - mode coupling and its impact on spatially multiplexed systems," in *Optical Fiber Telecommunications* (Optics and Photonics Series), 6th ed., I. P. Kaminow, T. Li, and A. E. Willner, Eds. Boston, MA, USA: Academic Press, 2013, pp. 491–568, iSSN: 15575837. [Online]. Available: https://www.sciencedirect.com/science/article/pii/B9780123969606000110

[20] S. O. Arik, J. M. Kahn, and K.-P. Ho, "MIMO signal processing for mode-division multiplexing: An overview of channel models and signal processing architectures," *IEEE Signal Process. Mag.*, vol. 31, no. 2, pp. 25–34, Mar. 2014. [Online]. Available: https://ieeexplore.ieee.org/abstract/document/6739233

[21] B. Collins and P. Sniady, "Integration with respect to the haar measure on unitary, orthogonal and symplectic group," *Commun. Math. Phys.*, vol. 264, no. 3, pp. 773–795, Jun. 2006. [Online]. Available: http://arxiv.org/abs/math-ph/0402073

Anirudh Vijay (Member, IEEE) received the B.Tech. and M.Tech. degrees in electrical engineering from the Indian Institute of Technology Madras, Chennai, India, in 2019, and the Ph.D. degree in electrical engineering from Stanford University, Stanford, CA, USA, in 2025. His research interests include optical communications, mode-division multiplexing, and data-center applications.

Nika Zahedi is currently working toward the B.S. and M.S. degrees in electrical engineering with Stanford University, Stanford, CA, USA. Her current research interests include mode-division multiplexing, signal processing, and optimization techniques.

Oleksiy Krutko (Member, IEEE) received the B.S. degree in electrical engineering from the University of Texas at Austin, Austin, TX, USA, in 2020, and the Ph.D. degree from Stanford University, Stanford, CA, USA, in 2025. His research interests include optical fiber communications and photonic devices.

Rebecca Refaee received the B.S. degree in mathematics and the M.S. degree in electrical engineering from Stanford University, Stanford, CA, USA in 2024. She is currently working toward the Ph.D. degree in electrical engineering with Stanford University. Her current research interests include optical communications and mode-division multiplexing.

Joseph M. Kahn (Life Fellow, IEEE) received the A.B., M.A. and Ph.D. degrees in physics from the University of California, Berkeley, Berkeley, CA, USA, in 1981, 1983 and 1986, respectively. From 1987 to 1990, he was with AT&T Bell Laboratories. In 1989, he demonstrated the first successful synchronous (i.e., coherent) detection using semiconductor lasers, achieving record receiver sensitivity. From 1990 to 2003, he was with the Electrical Engineering and Computer Sciences Faculty at Berkeley. In 2003, he became a Professor of electrical engineering in the E. L. Ginzton Laboratory with Stanford University, Stanford, CA, USA. He demonstrated coherent detection of QPSK in 1992. In 1999, D. S. Shiu and he has authored or coauthored the first work on probabilistic shaping for optical communications. In 1990 and early 2000, he and collaborators performed seminal work on indoor and outdoor free-space optical communications and multi-input multi-output wireless communications. In 2000, he and K. P. Ho founded StrataLight Communications, whose 40 Gb/s-per-wavelength long-haul fiber transmission systems were deployed widely by AT&T, Deutsche Telekom, and other carriers. In 2002, Ho and he applied to patent the first electronic compensation of fiber Kerr nonlinearity. StrataLight was acquired by Opnext in 2009. He and collaborators have extensively studied rate-adaptive coding and modulation, and digital signal processing for mitigating linear and nonlinear impairments in coherent systems. In 2008, E. Ip and he (and G. Li independently) invented simplified digital backpropagation for compensating fiber Kerr nonlinearity and dispersion. Since 2004, he and collaborators have been studied propagation, modal statistics, spatial multiplexing and imaging in multimode fibers, elucidating principal modes and demonstrating transmission beyond the traditional bandwidth-distance limit in 2005, deriving the statistics of coupled modal group delays and gains in 2011, and deriving resolution limits for imaging in 2013. His current research interests include optical frequency comb generators, coherent data center links, rate-adaptive access networks, fiber Kerr nonlinearity mitigation, ultra-long-haul submarine links, and optimal free-space transmission through atmospheric turbulence. He was the recipient of the National Science Foundation Presidential Young Investigator Award in 1991.